

# Temporal Evolution of flow in Porous Materials: From Homogenization to Instability

Ahmad Zareei, Deng Pan, and Ariel Amir\*

School of Engineering and Applied Sciences, Harvard University, Cambridge, MA, 02148

(Dated: March 17, 2021)

We study the dynamics of flow-networks in porous media using a pore-network model. First, we consider a class of erosion dynamics assuming a constitutive law depending on flow rate, local velocities, or shear stress at the walls. We show that depending on the erosion law, the flow may become uniform and homogenize, stay as it is, or become unstable and develop channels. By defining an order parameter capturing different behaviors we show that a phase transition occurs depending on the erosion dynamics. Using a simple model, we identify quantitative criteria to distinguish these regimes. Lastly, we show that pores clogging at the initial stages show analogous behaviors depending on clogging dynamics, however, due to the pore throat blockages and changes in the connections the evolution diverges from its initial trend.

do we show this? If not remove.

Fluid flow through a porous medium undergoing a dynamical change in its network of micro-structure is a challenging problem and has many environmental and industrial applications [1–14]. The disordered pore structure of a porous medium results in a heterogeneously distributed fluid flow between the pores. Due to the fluid flow, the pore structure can further change dynamically either through the erosion or pore boundary walls or deposition/sedimentation of material on the boundary of the pores. Such heterogeneous and dynamical changes of the solid structure affect the pore-level fluid flow which in turn affects the dynamical changes to the pore structure. This feedback mechanism along with the initial heterogeneous fluid flow complicates the dynamical process and makes it difficult to understand and predict the porous media behavior. Nonetheless, an understanding of the dynamical change is essential to improve any of the porous media applications where the pore network changes over time, applications such as groundwater remediation and precipitation of minerals in rocks [15], biofilm growth in water filtration, and protective filters [4–8], as well as enhanced oil recovery with polymer flooding [16, 17], or water-driven erosion [18, 19].

In light of the plethora of applications, it is surprising that the evolution of porous structures exposed to erosion and deposition has only been partially understood both theoretically and experimentally. In order to model erosion in porous materials, different models have been used where erosion is assumed to be locally proportional to different flow parameters. Some studies have focused on the erosion of the pore structure proportional to the shear stress at the walls [20–23], or proportional to the power dissipated by the flow [24–26]. More recently it has been shown using a coarse grained model and an erosion that depends on the pressure gradient branching instability has been observed [19, 27]. Similarly, in clogging, deposition rate based on local fluid flux, velocity, or even at a constant rate independent of any flow pa-

rameters has been used [28–30]. In order to unify the different approaches, we use a general continuous model which allows us to study the effect of different erosion or clogging dynamics with a single constitutive law. Additionally, we use a network approach [31–35] to study the flow dynamics in the porous media which gives us the advantage of not requiring any additional homogenization or mean-field approximation and at the same time allows us to simulate larger domains.

The network of pores inside the solid structure is connected together through pore throats that effectively show resistance to the fluid flow between the pores (Fig. 1a). In a network model, the pores/voids of the porous medium are represented by a two- or three-dimensional lattice of nodes. The edges between the nodes of the network represent the pore-throats between the pores and are modeled using cylindrical tubes characterized by their radius and length. Network-based models have successfully shown to capture key properties of fluid flow in a porous material such as the probability distribution of fluid flux [31], the permeability scaling during clogging [36], or the first fluidized path in a porous structure [37]. In order to study erosion in such network models, the degradation of the solid skeleton or clogging of pores is taken into account by the change (increase or decrease) in the resistance of the edges between the pores. Using a general local erosion law that can model different dynamics, we show a variety of behaviors are possible. The network can either move toward stability and homogenization, stay as it is with no significant change in network statistics, or even become unstable and develop channels. Using numerical solutions with an erosion model on a random network we show the emergence of two behaviors and morphologies are possible through selective erosion and subsequent flow enhancement. Using a simplified model we capture the underlying physics and furthermore show a phase transition occurs depending on the parameters of the model.

*Methods and Results*—We consider low-Reynolds fluid flow through the porous network, i.e.,  $\rho u^2 / \mu \ll 1$  where  $\rho$  is the fluid density and  $\mu$  is the kinematic viscosity,  $u$  and  $r$  are characteristic fluid velocity and pore radius.

to be consistent  
with the rest  
of the paper.

\* arielamir@seas.harvard.edu

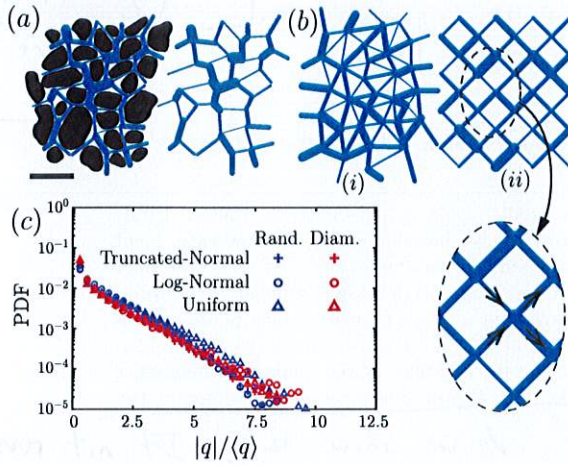


FIG. 1. (a) Cross section of a porous media obtained using computerized tomography (CT) scan of a sandstone sample (CT image taken from [38]). The scale in bottom left shows 1mm. The network of pores and throats is highlighted in blue. In the network model, the pores are represented with nodes and the throats between pores are approximated with tubes connecting the pores together. (b) Schematic of a topologically random network (i); and a structured diamond grid network (ii). The edge diameters in both networks are randomly distributed. The inset figure shows the conservation of mass at each node. (c) The universal probability distribution function (PDF) of fluid flux for a topologically random (in blue) or diamond network (red) with a highly disordered random net including uniform (triangles), log-normal (circles), and truncated normal (plus) distributions. The distribution parameters are chosen such that the coefficient of variation becomes 0.5 (highly disordered pore size). Generally, in a highly disordered random network, the PDF of normalized fluid flux becomes independent of the network and follows a universal distribution with an exponential tail.

In such conditions, the fluid flow in each tube follows the Poiseuille law  $p_i - p_j = (8\mu l_{ij}/\pi r_{ij}^4)q_{ij}$  where  $p_i, p_j$  represents pressures at neighboring nodes  $i, j$ , and  $r_{ij}, l_{ij}, q_{ij}$  are respectively the radius, length, and fluid flow rate at the edge connecting pores  $i$  and  $j$ . The coefficient  $\pi r_{ij}^4/8\mu l_{ij}$  which relates the fluid flux to the pressure difference can be considered as the conductance  $C_{ij}$  of the edge  $ij$  in the pore-network. In addition to Poiseuille flow at the edges, the total incoming flow at a node should be equal to the total outgoing flow in order to conserve mass. The conservation of mass at pore  $i$  can be written as  $\sum_{j \in \mathcal{N}(i)} q_{ij} = 0$  where  $\mathcal{N}(i)$  represents all the neighboring nodes of node  $i$ . First, we consider a topologically random network of nodes constructed using a uniform distribution of  $N_x \times N_y$  nodes in a planar domain  $[0, L_x] \times [0, L_y]$  where the nodes connectivity are obtained using Delaunay triangulation (see Fig. 1b for a part of such network). The radius of the edges are considered as independent and identically distributed random variables sampled from a probability distribution that can be either uniform, log-normal, or a truncated

normal distribution (see supplementary material S1 for more details). Assuming a pressure difference between the boundary nodes at the left and the right boundary, the pressure at the nodes, and the fluid flow rate at the tubes can be obtained by solving the corresponding set of linear equations. We find that for large enough randomness in the edge radii (i.e.,  $\text{std}(r_{ij})/\text{mean}(r_{ij}) > 0.5$ ), the PDF is well described by a single exponential distribution as shown in Fig. 1c. The exponential form of the PDF reflects the relatively small number of extremely large fluid flux. The exponential distribution of fluid flux obtained here is similar to the earlier experimental or numerical measurements [31, 36, 39]. Next we consider a structured diamond-grid of pores (Fig. 1b) which significantly simplifies the geometrical complexity of the network. First, we find that the PDF of normalized fluid flux remains unchanged in such networks for various distributions and in fact matches with an unstructured random network (Fig. 1c). The diamond grid allows us to analytically track the propagation of fluid into the network and calculate the distribution of fluid flux using a mean-field approximation (see supplementary material). Using a similar idea proposed for the force distribution in granular materials [40, 41], we find that the PDF of normalized fluid flux inside a highly disordered porous material converges to a universal distribution with an exponential form, i.e.,  $p(\hat{q}) \propto e^{-\alpha\hat{q}}$  for large  $\hat{q}$  where  $\hat{q}$  is the normalized fluid flux  $\hat{q} = q/\langle q \rangle$  (see supplementary materials S3). This result indicates that the diamond grid network of pores where cylindrical edges between the pores have a highly disordered distribution is enough to capture the statistics of a heterogeneous fluid flow inside a porous material.

In order to model erosion in porous media, we consider the abrasion in the throats which correspond to the change in the radius of the edges in the network. We model the dynamics of the change in the radius as

$$\frac{dr_{ij}}{dt} = \alpha \frac{q_{ij}}{r_{ij}^n} \quad (1)$$

where  $n$  is an integer number and  $c$  is a constant. Different powers of  $n$  correspond to different physics in the erosion. Particularly, when (i)  $n = 0$  the erosion depends on the amount of flux  $q_{ij}$  passing through the edge; (ii)  $n = 2$  the erosion depends on the local velocities; (iii)  $n = 3$  the erosion depends on the shear force at the boundary of the throat. We consider the diamond-grid network initialized with a size of  $N_x \times N_y$  tubes in the horizontal and vertical directions. We initialize the network with a uniform random distribution of diameters within  $[r_{\min}, r_{\max}]$  range with a large coefficient of variation such that  $\sigma_r/r_0 \approx 0.5$  where  $\sigma_r$  is the standard deviation, and  $r_0 = \langle r \rangle$ . The flow inside the pores, PDF of flux in the tubes, and PDF of tube radii are shown in Fig. 2. We assume a constant pressure difference between the left and the right boundaries. In each time step, we increase the local radius of the tubes based on the erosion law introduced in Eq. (1). Note that  $r_{ij}(t+1) = r_{ij}(t) + (\alpha\delta t)q_{ij}(t)/r_{ij}^n(t)$ , where the coefficient  $\alpha\delta t$  is chosen such that the maximum change

W:KA about 30%?

1b (i)

ed, ps  
vir

1b (i)

S3

+ sim

2  
Right  
we  
switched  
?

Can be removed / moved  
to SI if we  
need SI.

in the radius at each time step is smaller than one-tenth of the smallest tube's radius i.e.  $\max(\Delta r_{ij}) \leq r_{\min}/10$  of the smallest radius at the initial configuration. This condition guarantees that at each step a small amount of material is eroded and there's no sudden change in the network. We further test that decreasing  $\max(\Delta r_{ij})$  to half and we observe that the average relative change in the flux vector becomes 1.2%, and the PDFs remain intact without any change. We continue the simulations to until  $\langle r \rangle = 2r_0$ . The results of the simulations for

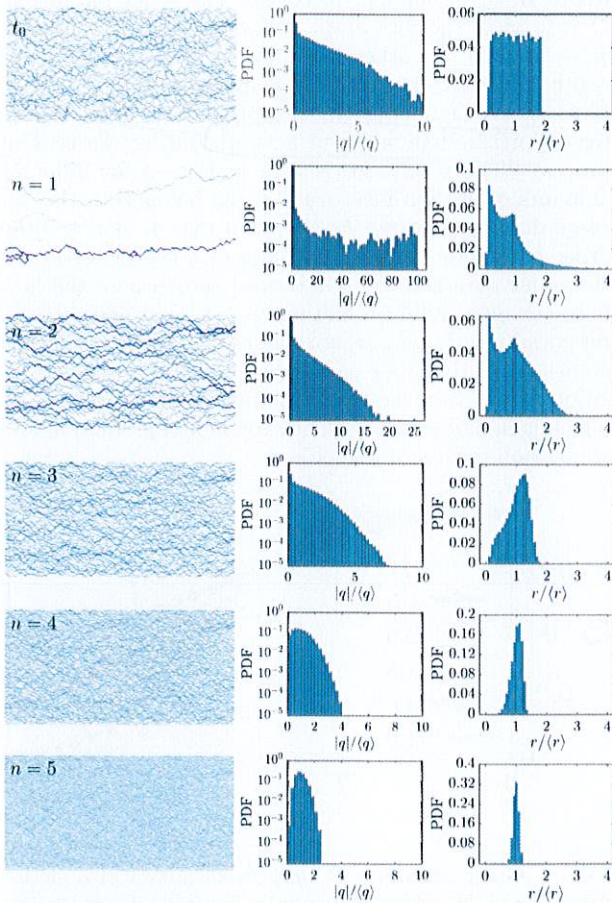


FIG. 2. Erosion in a network of pipes. The initial condition is shown with the label  $t = 0$  in the first row. Each row afterward corresponds to the simulation result after  $N$  steps such that  $\langle r_{t=N} \rangle = 2r_0$  where  $r_0 = \langle r_{t=0} \rangle$  or twice the initial average radius, as a result in all cases the same amount of material is eroded. The erosion law is based on Eq. (1) where different powers of  $n$  correspond to different models of erosion. The first column is a snapshot of the pore network, the second column is the PDF of normalized fluid flux  $|q|/\langle q \rangle$ , and the last column is the PDF of normalized radius  $r/\langle r \rangle$ .

different  $n$  are shown in Fig. 2. When  $n = 1$  or  $2$ , the network develops channels. In such cases, the flow is dominated by a few edges carrying most of the flow while the rest of the network carries almost no flow. This can be seen in the PDF of the normalized radius distribu-

tion which becomes bimodal. Furthermore, the PDF of the normalized fluid flux contain a small number of edges with very large flux values while the majority of the edges carry small flux. Contrary to  $n = 1, 2$ , when  $n = 3$  and the erosion depends on shear at the throats' boundary walls, we find that the flow patterns stay very close to the initial shape, however, with larger and exacerbated flux values. Although the maximum fluid flux increases, the PDF of normalized fluid fluxes remains almost exponential, and the PDF of diameters moves toward larger values. Increasing  $n$  to larger values,  $n = 4$  or  $5$ , we find that the flow pattern in the network moves toward homogenization. Here, the tail of the normalized fluid flux distribution retracts and the distribution moves toward the average value. We further find that the PDF of the diameters moves toward the average and the coefficient of variation reduces. Running the simulations for longer times, we observe that the flow becomes completely uniform where only a single radius appears to carry the flow with the same fluid flux (i.e., the average value) for all the tubes in the network. In summary, we have observed a transition in the network behavior during erosion which happens at  $n = 3$ : when  $n < 3$  the network moves toward developing channels, and when  $n > 3$  the erosion results in the homogenization of the flow.

*Simplified Model*— In order to understand the underlying reason behind the transition in network behavior during erosion for different powers of  $n$ , we focus on a simplified model with only two tubes in parallel or series (see Fig. 3a,b). First, assuming two cylindrical tubes with radii  $r_1, r_2$  in series and connected back to back, the flow is the same for the two tubes  $q_1 = q_2 = q$  (Fig. 3a). The radius of each tube then changes with  $dr_i/dt = \alpha q/r_i^n$  where  $i = 1, 2$ . Each tube can be considered as a resistor where its conductivity  $C_i = \pi r_i^4/8\mu l_i$  changes over time. In similarity with resistor networks, the pressure difference  $\Delta P$  acts analogous to the voltage difference and the fluid flux  $q$  becomes analogous to the current where we have  $q = C_i \Delta P_i$ . When the cylindrical tubes are in series, we find that the conductivity of each tube changes as  $dC_i/dt \propto C^{(n-3)/4}$ . As a result, each tube's conductivity increases with a rate depending on  $n$ , i.e. the larger the  $n$  the faster it moves toward larger values. If we consider the pressure at the junction between tubes, we find that this middle point pressure moves toward the average value of pressure on both sides (see Fig. 3a1). As a result, when the tubes are in series, the erosion results in a homogenized distribution of pressure. Contrary to tubes in series, when the tubes are in parallel (Fig. 3b), the flow divides between the two tubes based on their conductivity i.e.  $q_1/q_2 = C_1/C_2$ . Since each tube's radius changes as  $dr_i/dt = \alpha q_i/r_i^n$ , the evolution of the fluid flow ratio becomes

$$\frac{d}{dt} \left( \frac{C_1}{C_2} \right) \propto \frac{C_1}{C_2^{(n+1)/4}} \left( \left( \frac{C_1}{C_2} \right)^{\frac{n-3}{4}} - 1 \right). \quad (2)$$

When  $n = 3$  in Eq. (2), the right-hand-side becomes zero and as a result the flow ratio  $C_1/C_2$  remains con-

stant and does not change. However, when  $n \neq 3$ , we find that  $C_1/C_2 = 1$  is an equilibrium point. When  $n > 3$  this equilibrium solution is stable and the flow moves toward homogenization; however, when  $n < 3$  this equilibrium solution becomes unstable and the solution moves toward  $C_1/C_2 \rightarrow 0$  or  $\infty$  which means that the whole flow passes through one of the tubes. To summarize, when the tubes are in series any erosion law makes flow become more uniform; however, when the tubes are in parallel depending on the power  $n$  the flow in the tubes can move toward becoming more uniform ( $n > 3$ ), stay the same ( $n = 3$ ), or move toward instability and channel development ( $n < 3$ ). Since a complex network includes both series and parallel connections, we expect that the whole network structure behaves in a similar manner and we observe a network transition between becoming uniform ( $n < 3$ ) to developing channels ( $n > 3$ ). This observation here is consistent with the numerical simulation results shown in Fig. 2.

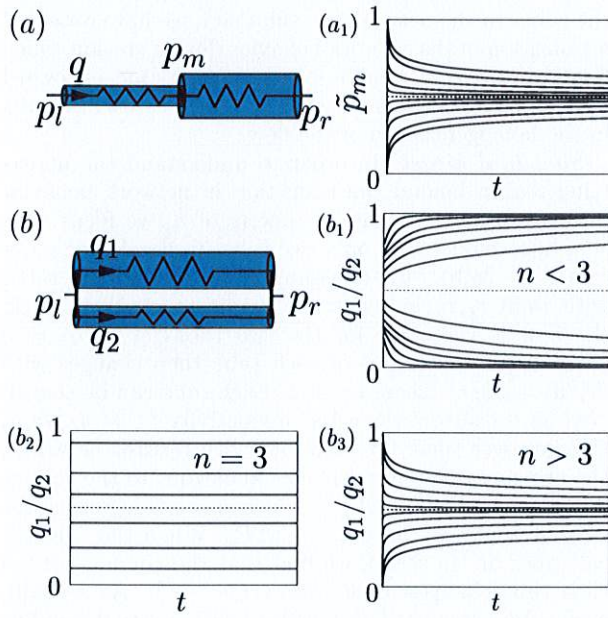


FIG. 3. Two tubes in (a) series or (b) parallel configuration. When the tubes are in series configuration, the tubes have the same fluid flow rate  $q$ . The tube radius dynamically change with the erosion law  $\dot{r}_i \propto q/r_i^n$ . For any  $n$ , the normalized pressure at the junction between the tubes  $\tilde{p}_m = (p_m - p_l)/(p_r - p_l)$  approaches  $1/2$  which results in a homogenized pressure distribution shown in (a<sub>2</sub>). When the pipes are in parallel, however, the flow is distributed among the tubes based on their flow conductivity  $C_1, C_2$ . The local fluid flow rate then affects the erosion of the tub  $\dot{r}_i \propto q_i/r_i^n$ . When  $n < 3$  in the erosion law, the fluid flow eventually passes through a single tube, and channeling occurs. (b<sub>2</sub>) when  $n = 3$ , the flow ratio between the pipes does not change, and (b<sub>3</sub>) when  $n > 3$  the flow ratio approaches  $1/2$  which is the homogenization.

*Phase transition*—order to quantify the transition of

the network between channeling instability and homogenization, we define an order parameter  $\mathcal{O}$  that moves toward 0 or 1 if the network moves toward channeling or homogenization respectively. The order parameter is defined as

$$\mathcal{O} = \frac{1}{N-1} \left( N - \frac{\left( \sum_{ij} q_{ij}^2 \right)^2}{\sum_{ij} q_{ij}^4} \right) \quad (3)$$

where  $N$  is the number of edges. The order parameter  $\mathcal{O} = 0$  when the flux in all the edges become the same  $q_{ij} = \bar{q}$ . On the other hand, when fluid flux becomes highly localized with only a few edges with non-zero flux,  $\mathcal{O} \rightarrow 1$ . We numerically calculated the order parameter  $\mathcal{O}$  for the diamond-grid network during the erosion process. The results are shown in Fig. 4 for different amounts of erosion measured by the increase in the average diameter  $\langle r \rangle / r_0$ . As shown in Fig. 4, at  $n = 3$  the order parameter remains unchanged; however for  $n > 3$  the order parameter moves toward zero, where the flow becomes more uniform and for  $n < 3$  the order parameter goes toward unity, where channels are developed. The transition in the order parameter indicates a phase transition at  $n = 3$  in the long time behavior of the network which is in agreement with the toy model prediction and simulation results of Fig. 2.

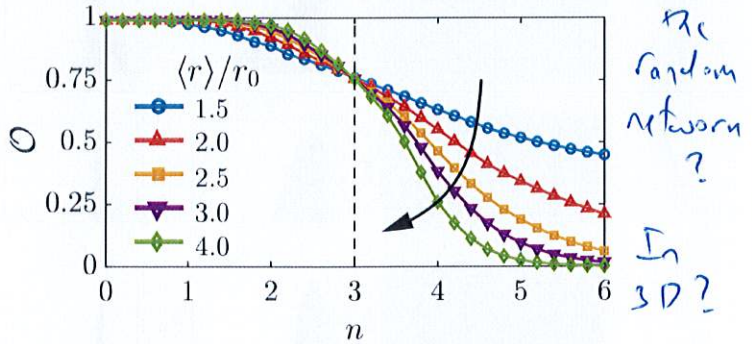


FIG. 4. Order parameter  $\mathcal{O}$  for different powers of  $n$  plotted over time as the network structure is eroded and average edge radius is increasing  $\langle r \rangle / r_0$ . When  $n < 3$  the order parameter increases ( $\mathcal{O} \rightarrow 1$ ) while the network is developing channels, and when  $n > 3$  the order parameter decreases ( $\mathcal{O} \rightarrow 0$ ) while the network moves toward homogenization, and when  $n = 3$  the order parameter stays as it while the network statistics remains unchanged.

*Clogging Dynamics*—Besides erosion, another change in the network is the deposition/sedimentation of material on the boundary walls of the porous material. We name this dynamical change a “clogging” process as opposed to erosion. Contrary to erosion, the clogging behavior may cause some edges to block which effectively alters the network of connectivity and network behavior. This change in the connection between nodes through edges getting blocked can drastically alter porous struc-

ture behavior, e.g., causes a huge difference between effective and true porosity [36]. Despite the drastic change of network with blockages, we can still focus on the *initial* change in the order parameter. The derivative of order parameter can be written as

$$\frac{d\mathcal{O}}{dt} = \sum_{ij} \sum_{kl} \frac{\partial \mathcal{O}}{\partial q_{ij}} \frac{\partial q_{ij}}{\partial C_{kl}} \frac{\partial C_{kl}}{\partial t} \quad (4)$$

where the last term changes sign from erosion to clogging, i.e.,  $\partial C_{kl}/\partial t = \pm \alpha \pi q_{kl}/r_{kl}^{n-3} \mu l_{kl}$  for erosion and clogging respectively. As a result, the magnitude of change in the order parameter equals to that of erosion. Note that in Eq. (4), the second term depends on the network topology and pore throat clogging results in the change of network topology at later times. In short times, however, similar to the erosion, a phase transition exists at  $n = 3$ . When  $n < 3$  the network moves toward homogenization during the clogging process and when  $n > 3$  the flow moves toward the development of channeling instability. This initial direction, however, might not hold true due to the aforementioned complex changes in the connectivity

network during the clogging process.

*Conclusion*—In summary, we analyzed the dynamics of the porous networks during erosion. We showed that depending on different erosion laws various network behaviors are observable. We used simple erosion laws, inspired by previously proposed models, and showed that depending on the rate of erosion the network can either move toward homogenization or toward developing a channeling instability. Next, we propose an order parameter to

capture the phase transition behavior, and using a simplified model of two tubes we elucidated the physical origin of the phase transition behavior. In the case of clogging, since the network connectivity can vary significantly our approach does not hold at large times, however, the initial variation can be captured using our model where the results similarly show a behavior change at  $n = 3$ . Our results signifies the importance of local dynamics and feedback mechanism in long time global behavior and complements similar feedback induced studies for active conducting mediums [42].

*Acknowledgments*—We would like to acknowledge Kavli Institute for the discussions and also MRSEC DMR-2011754 for the support.

+ Old  
MRSEC

Dily  
Shu,  
Dilip

✓

U.S. 2015 MT

- [1] D. Fragedakis, C. Kouris, Y. Dimakopoulos, and J. Tsamopoulos, *Physics of Fluids* **27**, 082102 (2015).
- [2] M. Sahimi, *Flow and transport in porous media and fractured rock: from classical methods to modern approaches* (John Wiley & Sons, 2011).
- [3] W. H. Schlesinger, *Science* **284**, 2095 (1999).
- [4] J. Herzig, D. Leclerc, and P. L. Goff, *Industrial & Engineering Chemistry* **62**, 8 (1970).
- [5] C. Tien and A. C. Payatakes, *AICHE Journal* **25**, 737 (1979).
- [6] D. P. Jaisi, N. B. Saleh, R. E. Blake, and M. Elimelech, *Environmental Science & Technology* **42**, 8317 (2008).
- [7] M. Carrel, V. L. Morales, M. A. Beltran, N. Derlon, R. Kaufmann, E. Morgenroth, and M. Holzner, *Water Research* **134**, 280 (2018).
- [8] J. D. Seymour, J. P. Gage, S. L. Codd, and R. Gerlach, *Physical Review Letters* **93**, 198103 (2004).
- [9] M. Duduta, B. Ho, V. C. Wood, P. Limthongkul, V. E. Brunini, W. C. Carter, and Y.-M. Chiang, *Advanced Energy Materials* **1**, 511 (2011).
- [10] H. Sun, J. Zhu, D. Baumann, L. Peng, Y. Xu, I. Shakir, Y. Huang, and X. Duan, *Nature Reviews Materials* **4**, 45 (2019).
- [11] S. Marbach, K. Alim, N. Andrew, A. Pringle, and M. P. Brenner, *Physical Review Letters* **117**, 178103 (2016).
- [12] A. Tero, S. Takagi, T. Saigusa, K. Ito, D. P. Bebbert, M. D. Fricker, K. Yumiki, R. Kobayashi, and T. Nakagaki, *Science* **327**, 439 (2010).
- [13] K. Alim, G. Amselem, F. Peaudecerf, M. P. Brenner, and A. Pringle, *Proceedings of the National Academy of Sciences* **110**, 13306 (2013).
- [14] L. L. Heaton, E. López, P. K. Maini, M. D. Fricker, and N. S. Jones, *Proceedings of the Royal Society B: Biological Sciences* **277**, 3265 (2010).
- [15] M. N. Rad, N. Shokri, and M. Sahimi, *Physical Review E* **88**, 032404 (2013).
- [16] L. W. Lake, R. Johns, B. Rossen, G. A. Pope, et al., *Fundamentals of Enhanced Oil Recovery*, (2014).
- [17] S. Parsa, E. Santanach-Carreras, L. Xiao, and D. A. Weitz, *Physical Review Fluids* **5**, 022001 (2020).
- [18] N. Schorghofer, B. Jensen, A. Kudrolli, and D. H. Rothman, *Journal of Fluid Mechanics* **503**, 357 (2004).
- [19] A. Mahadevan, A. Orpe, A. Kudrolli, and L. Mahadevan, *EPL (Europhysics Letters)* **98**, 58003 (2012).
- [20] R. Jäger, M. Mendoza, and H. J. Herrmann, *Physical Review E* **95**, 013110 (2017).
- [21] L. Ristroph, M. N. Moore, S. Childress, M. J. Shelley, and J. Zhang, *Proceedings of the National Academy of Sciences* **109**, 19606 (2012).
- [22] W. Hacking, E. VanBavel, and J. Spran, *American Journal of Physiology-Heart and Circulatory Physiology* **270**, H364 (1996).
- [23] C. F. Wan and R. Fell, *Journal of Geotechnical and Environmental engineering* **130**, 373 (2004).
- [24] H. Steeb, S. Diebel, and I. Vardoulakis, “Modeling internal erosion in porous media,” in *Computer Applications In Geotechnical Engineering*, pp. 1–10.
- [25] D. Marot, V. D. Le, J. Garnier, L. Thorel, and P. Audrain, *European Journal of Environmental and Civil Engineering* **16**, 1 (2012).
- [26] L. Siblette, F. Lominé, P. Poullain, Y. Sail, and D. Marot, *Hydrological Processes* **29**, 2149 (2015).
- [27] N. J. Derr, D. C. Fronk, C. A. Weber, A. Mahadevan, C. H. Rycroft, and L. Mahadevan, *Physical Review Letters* **125**, 158002 (2020).
- [28] H. Yang and M. T. Balhoff, *AICHE Journal* **63**, 3118 (2017).
- [29] L. N. Reddi, X. Ming, M. G. Hajra, and I. M. Lee, *Jour-*

- nal of Geotechnical and Geoenvironmental Engineering **126**, 236 (2000).
- [30] G. Boccardo, D. L. Marchisio, and R. Sethi, Journal of Colloid and Interface Science **417**, 227 (2014).
- [31] K. Alim, S. Parsa, D. A. Weitz, and M. P. Brenner, Physical Review Letters **119**, 144501 (2017).
- [32] I. Fatt *et al.*, Transactions of the AIME **207**, 144 (1956).
- [33] M. J. Blunt, B. Bijeljic, H. Dong, O. Gharbi, S. Iglauer, P. Mostaghimi, A. Paluszny, and C. Pentland, Advances in Water resources **51**, 197 (2013).
- [34] N. Stoop, N. Waisbord, V. Kantsler, V. Heinonen, J. S. Guasto, and J. Dunkel, Journal of Non-Newtonian Fluid Mechanics **268**, 66 (2019).
- [35] S. L. Bryant, P. R. King, and D. W. Mellor, Transport in porous media **11**, 53 (1993).

↳ 2024  
reference

???

- [36] S. Parsa, A. Zareei, E. Santanach-Carreras, E. Morris, A. Amir, L. Xiao, and D. A. Weitz, arXiv (2021).
- [37] ~~911.~~
- [38] L. T. Akanji and S. K. Matthai, Transport in Porous Media **81**, 241 (2010).
- [39] S. S. Datta, H. Chiang, T. Ramakrishnan, and D. A. Weitz, Physical Review Letters **111**, 064501 (2013).
- [40] C.-h. Liu, S. R. Nagel, D. Schecter, S. Coppersmith, S. Majumdar, O. Narayan, and T. Witten, Science **269**, 513 (1995).
- [41] S. Coppersmith, C.-h. Liu, S. Majumdar, O. Narayan, and T. Witten, Physical Review E **53**, 4673 (1996).
- [42] S. A. Ocko and L. Mahadevan, Physical Review Letters **114**, 134501 (2015).

# Temporal Evolution in the Networks of Porous Materials: From Homogenization to Instability

Ahmad Zareei, Pan Deng, and Ariel Amir\*

*School of Engineering and Applied Sciences, Harvard University, Cambridge, MA, 02148*

(Dated: March 17, 2021)

## S1. SIMULATION ALGORITHM

In our simulations, we tested two types of network: a (i) diamond-grid network, and a (ii) topologically random network. In the diamond-grid network, we choose  $N_x = 200$  edges in the horizontal direction and  $N_y = 100$  edges in the vertical direction. The random network is created using uniformly distributed points with on average  $N_x \times N_y$  edges in the horizontal and vertical directions. Note that the randomly distributed points are connected using Delaunay triangulation. The diameter of each edge is sampled from either a uniform distribution in  $r \in [1, 14]$ , log-normal distribution with  $\mu = 3, \sigma = 0.48$ , or truncated normal distribution with  $\mathcal{N}(\mu = 7.0, \sigma = 3.6)$ . The external flow pressure is applied horizontally from left to right. An external pressure is then considered between the left most nodes and the right most nodes ( $p_{\text{left}} = 10, p_{\text{right}} = 0$ ). Assuming a Poiseuille flow in each edge, the fluid flow  $q$  and pressure difference  $\delta P_e$  in each edge is related through  $q_e = C_e \delta P_e$ , where  $C_e = \pi r_e^4 / 8\mu L_e$ ,  $L_e$  is the length of the tube, and  $\mu$  is the viscosity of the fluid. Let  $\Delta$  be the transpose of the network's oriented incidence matrix. Note that the orientation of each edge is arbitrary since it only determines the positive direction of flow in that edge. Define  $|q_e\rangle$  as the vector of flow through all the edges, then we have  $|q_e\rangle = C_e \Delta |P_n\rangle$  where  $|P_n\rangle$  is the vector of pressure at all the nodes. With a given boundary condition, we solve the equation through a modified nodal analysis as follows. The conservation of mass at each node can be written as

$$|q_n\rangle = \Delta^\top \mathbf{C} \Delta |P_n\rangle, \quad (\text{S1})$$

where  $\mathbf{C} = \text{diag}(C_e^{(1)}, C_e^{(2)}, \dots, C_e^{(N_e)})$  is a diagonal matrix of edge conductances, and  $|q_n\rangle$  is the vector of total incoming flow to each node. Note that total incoming flow to an internal node is zero inside the network due to the conservation of mass, and is only non-zero at the boundary nodes. Renumbering the boundary nodes to be nodes 1 to  $N_B$ , we can partition Eq. (S1) to obtain

$$\begin{bmatrix} \Delta_b^\top \mathbf{C} \Delta_b & \Delta_b^\top \mathbf{C} \Delta_n \\ \Delta_n^\top \mathbf{C} \Delta_b & \Delta_n^\top \mathbf{C} \Delta_n \end{bmatrix} \begin{bmatrix} P_1^{BC} \\ P_2^{BC} \\ \vdots \\ P_{N_B}^{BC} \\ \hline P_{N_B+1} \\ \vdots \\ P_{N_n} \end{bmatrix} = \begin{bmatrix} q_1^{BC} \\ q_2^{BC} \\ \vdots \\ q_{N_B}^{BC} \\ \hline 0 \\ \vdots \\ 0 \end{bmatrix} \rightarrow \begin{bmatrix} \mathbf{A}_{bb} & \mathbf{A}_{bn} \\ \mathbf{A}_{nb} & \mathbf{A}_{nn} \end{bmatrix} \begin{bmatrix} P_1^{BC} \\ P_2^{BC} \\ \vdots \\ P_{N_B}^{BC} \\ \hline P_{N_B+1} \\ \vdots \\ P_{N_n} \end{bmatrix} = \begin{bmatrix} q_1^{BC} \\ q_2^{BC} \\ \vdots \\ q_{N_B}^{BC} \\ \hline 0 \\ \vdots \\ 0 \end{bmatrix} \quad (\text{S2})$$

where  $\mathbf{A}_{st} = \Delta_s^\top \mathbf{C} \Delta_t^\top$  and  $s, t \in \{a, b\}$ . In summary the above equations simplifies to

$$\begin{cases} \mathbf{A}_{bb}|P_{BC}\rangle + \mathbf{A}_{bn}|P\rangle = |q_{BC}\rangle \\ \mathbf{A}_{nb}|P_{BC}\rangle + \mathbf{A}_{nn}|P\rangle = 0 \end{cases} \quad (\text{S3})$$

Solving the above equation results in the pressure field on the nodes and the fluid flux at the boundary nodes. With the solution of  $q_e$ , the increase (decrease) of tube radius under erosion (clogging) law is

$$\frac{dr_e}{dt} \propto \pm \frac{q_e}{r_e^n}. \quad (\text{S4})$$

We use simple forward Euler to integrate the equations. For each iteration, we choose the time step  $dt$  so that  $\max(dr) = 0.1r_0$ , where  $r_0$  is the smallest radius among all edges.

---

\* arielamir@seas.harvard.edu



## S2. ADDITIONAL NUMERICAL RESULT

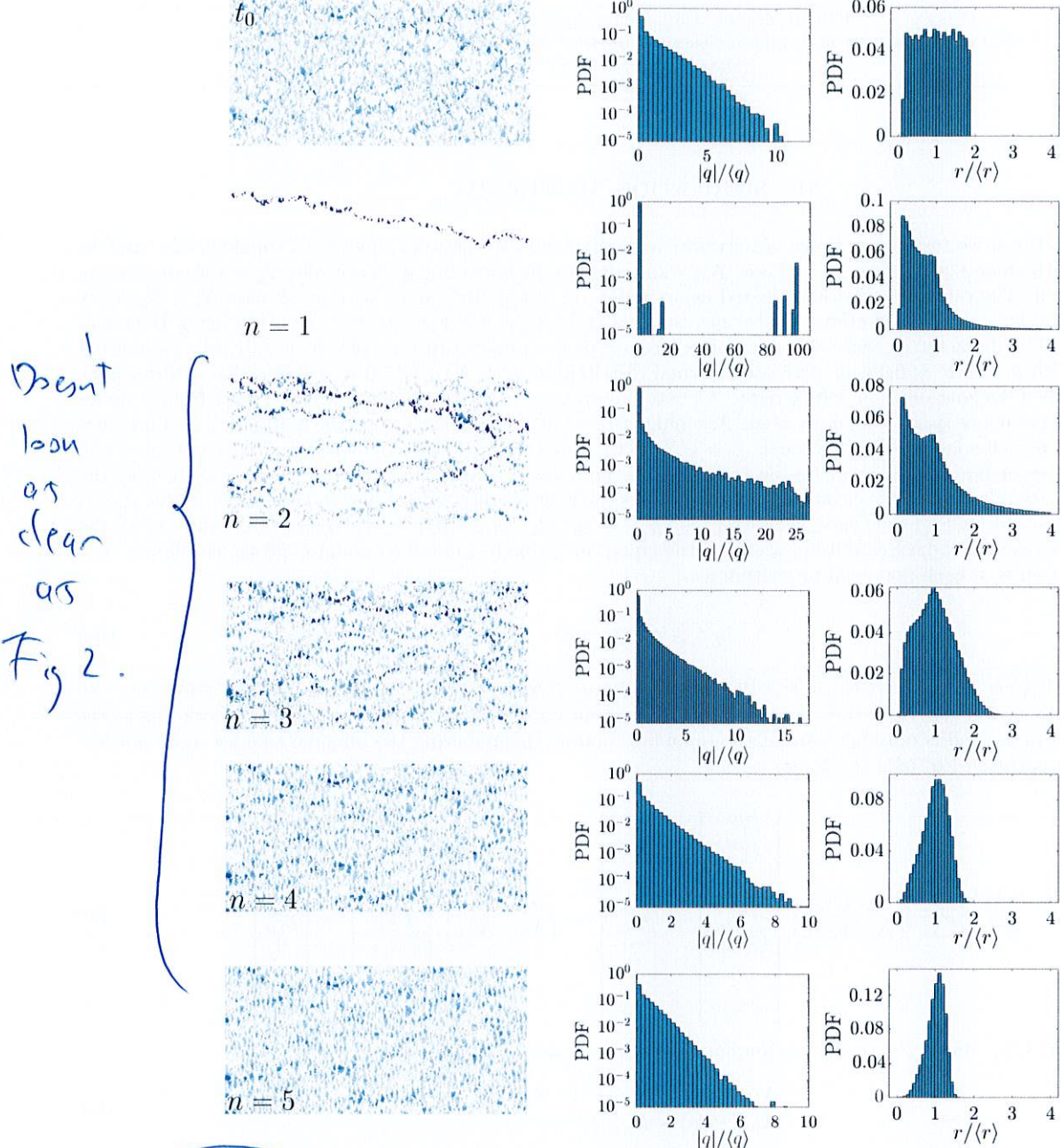


FIG. S1. Ahmad's version' Erosion in a topologically random network of pipes. The initial condition is shown with the label  $t = 0$  in the first row. Each row afterward corresponds to the simulation result after  $N$  steps such that  $\langle r_{t=N} \rangle = 2r_0$  where  $r_0 = \langle r_{t=0} \rangle$  or twice the initial average radius. The erosion law is based on Eq. (1) in the main text where different powers of  $n$  correspond to different models of erosion. The first column is a snapshot of the pore network, the second column is the PDF of normalized fluid flux  $q/\langle q \rangle$ , and the last column is the PDF of normalized radius  $r/\langle r \rangle$ .

## S3. ANALYTICAL RESULTS

true i, general  
principle.

As described in the main text, the PDF of flow in a topologically disordered network of tubes is the same as a structured diamond grid when the radius of the tubes have a highly disordered random distribution. In this section we show that the observed exponential distribution of fluid flux can be described using a random distribution of the diameters along with the conservation of mass in the network. In a diamond grid, the incoming flow to a node is redistributed among the outgoing edges (fluid flux is conserved). Due to the randomness of the tubes, one can imagine that the redistribution of the flow one node between the edges is a random itself and the only condition is that the fluid flux should be conserved. This model for the flow can be mapped one to one to the problem of force fluctuations in a bead pack [1, 2] as shown in Fig. S2. In a bead pack the force at each layer is redistributed to the next layer where the total force exerted on the next layer should be in equilibrium with the previous layer. Given the above

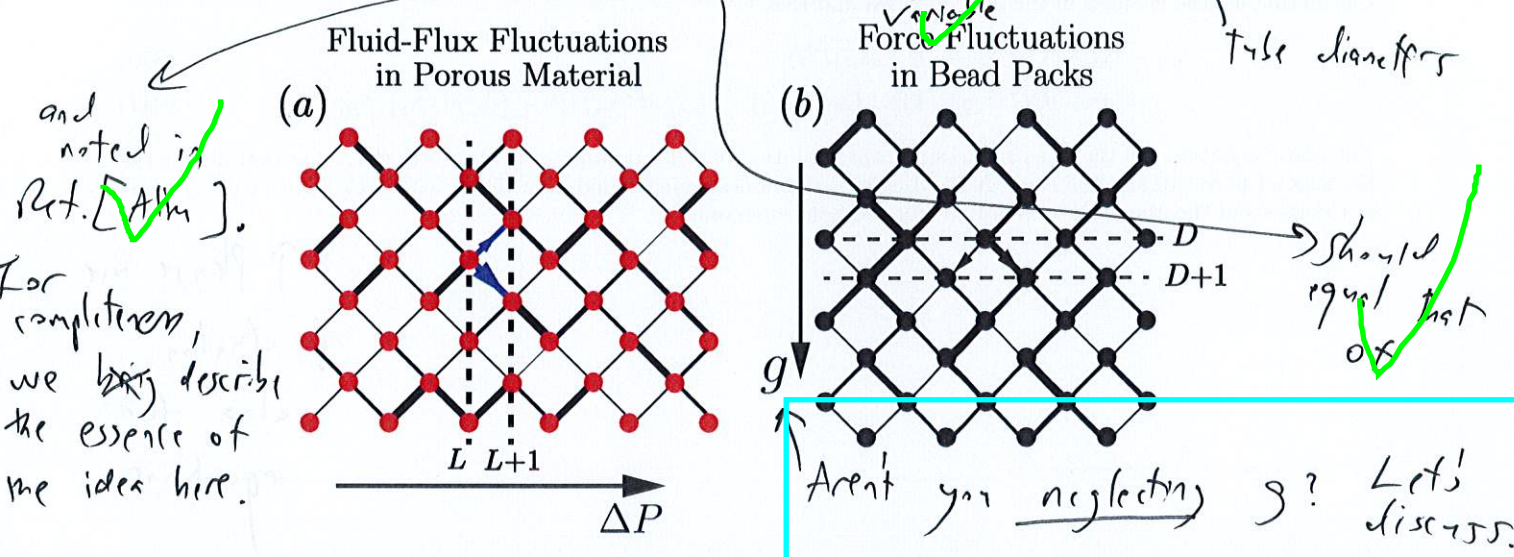


FIG. S2. (a) Schematic of diamond grid network of tubes. The incoming flow to each node is redistributed among the outgoing edges. The thickness of the lines shows the amount of fluid flux. (b) Schematic diagram showing beads (represented with nodes) and their contacts to the neighboring sites shown in the edges. The thickness of the edges show the weight transferred with that contact.

conditions, the flow at layer  $L + 1$  at node  $j$  can be obtained as

$$q(L+1,j) = \sum_i w_{ij} q(L,i) = w_{i,i+1} q(L,i+1) + w_{i,i} q(L,i), \quad (S5)$$

where  $w_{ij}$  shows the weights by which the flow is redistributed. Note that since the total fluid flux is conserved, then  $\sum_j w_{ij} = 1$ . Assuming a general distribution of  $\eta(w)$ , we can use the mean-field approximation to find the distribution of  $q$  at the layer  $L$ , i.e.,  $p_L(q)$ . The values of  $q(L,i)$  are not independent for neighboring sites; however, in our mean field approximation we ignore such correlations. We find

$$p_L(q) = \prod_{j=1}^N \left\{ \int_0^1 dw_j \eta(w_j) \int_0^\infty dq_j p_{L-1}(q_j) \right\} \times \delta \left( \sum_j w_j q_j - q \right) \quad (S6)$$

q's from, nicely satisfied via

The constraint that  $q$ 's emanating downward should add up to one is ~~X~~ the definition of  $\eta(w)$ . The only approximation in the above equation is that we neglect the possible correlation between the values of ~~X~~ among ancestors. If we take the Laplace transform of the above equation and define  $\tilde{p}(s) \equiv \int_0^\infty p(q) e^{-qs} dq$  we obtain

$$\tilde{P}(s) = \left( \int_0^1 dw \eta(w) \tilde{P}(sw) \right)^N \quad (S7)$$

Note that in the above equation  $N$  determines the number of neighboring sites and in our structured diamond grid  $N = 2$ . The above equation recursively converges to a distribution. The solution to the above recursive equation for two neighboring sites (diamond grid) becomes  $p(q) = 4q \exp(-2q)$  [1-3], which is a distribution with an exponential tail.

I am not sum what that means.

I don't think that's true.  
See Eq. 2.31  
in Ref [2]

Or simply use  $N=2$ ?

#### S4. CLOGGING BEHAVIOR AT INITIAL TIMES

Considering a small change in the radius of edges, and as a result the conductance of the edges  $\mathbf{C} + \delta\mathbf{C}$ , using Eq. (S3) we find that

$$|P'\rangle = |P\rangle - (\Delta_n^\top \mathbf{C} \Delta_n)^{-1} [(\Delta_n^\top \delta\mathbf{C} \Delta_n) |P\rangle + (\Delta_n^\top \delta\mathbf{C} \Delta_b) |P_{BC}\rangle], \quad (\text{S8})$$

where we used the fact that for an invertible matrix  $\mathbf{A}$  we have

$$(\mathbf{A} + \delta\mathbf{A})^{-1} = \mathbf{A}^{-1} - (\mathbf{A}^{-1} \delta\mathbf{A}) \mathbf{A}^{-1} + (\mathbf{A}^{-1} \delta\mathbf{A})^2 \mathbf{A}^{-1} + \dots \quad (\text{S9})$$

Calculating for the changes in the fluid flux, we find that

$$|q'\rangle = (\mathbf{C} + \delta\mathbf{C})(\Delta_b |P_{BC}\rangle + \Delta_n |P'\rangle) \quad (\text{S10})$$

$$= |q\rangle + \delta\mathbf{C}\mathbf{C}^{-1}|q\rangle - \mathbf{C}\Delta_n (\Delta_n^\top \mathbf{C} \Delta_n)^{-1} [(\Delta_n^\top \delta\mathbf{C} \Delta_n) |P\rangle + (\Delta_n^\top \delta\mathbf{C} \Delta_b) |P_{BC}\rangle]. \quad (\text{S11})$$

The above equation can then be used to study the evolution of order parameter in the networks. Note that during the blockage of pore-throats, the connectivity between the nodes changes and as a result network's connectivity matrix  $\Delta$  changes and the above approximation will not hold anymore.

↑ *Physical system*  
*problematic*  
*a lot for*  
*equations.*

- 
- [1] C.-h. Liu, S. R. Nagel, D. Schecter, S. Coppersmith, S. Majumdar, O. Narayan, and T. Witten, Force fluctuations in bead packs, *Science* **269**, 513 (1995).
  - [2] S. Coppersmith, C.-h. Liu, S. Majumdar, O. Narayan, and T. Witten, Model for force fluctuations in bead packs, *Physical Review E* **53**, 4673 (1996).
  - [3] K. Alim, S. Parsa, D. A. Weitz, and M. P. Brenner, Local pore size correlations determine flow distributions in porous media, *Physical Review Letters* **119**, 144501 (2017).

✓

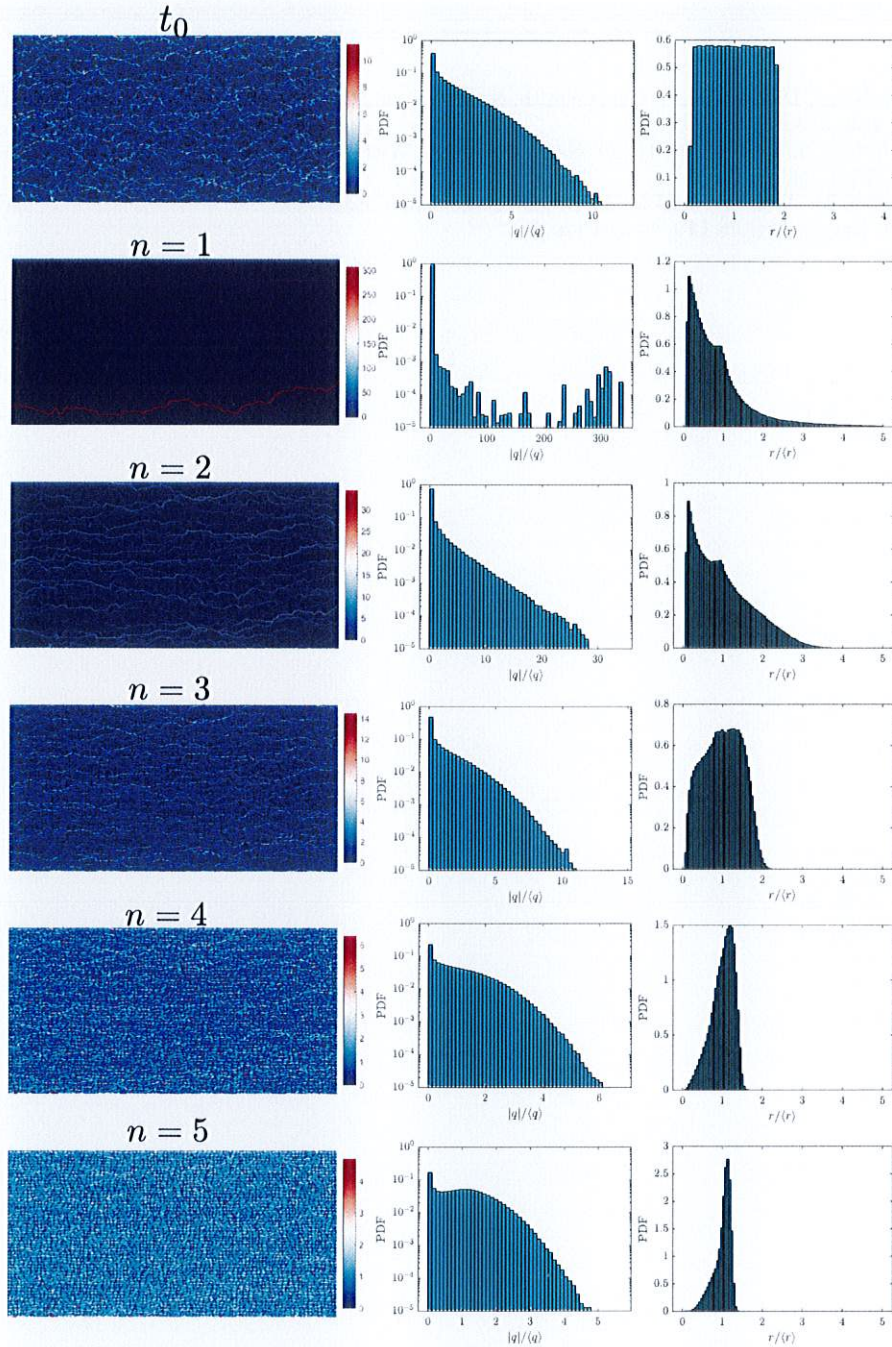


FIG. S3. Deng's version: Erosion in a topologically random network of pipes. The initial condition is shown with the label  $t = 0$  in the first row. Each row afterward corresponds to the simulation result after  $N$  steps such that  $\langle r_{t=N} \rangle = 2r_0$  where  $r_0 = \langle r_{t=0} \rangle$  or twice the initial average radius. The erosion law is based on Eq. (1) in the main text where different powers of  $n$  correspond to different models of erosion. The first column is a snapshot of the pore network, the second column is the PDF of normalized fluid flux  $|q|/\langle q \rangle$ , and the last column is the PDF of normalized radius  $r/\langle r \rangle$ .